Role of mechanical factors in cortical folding development

Mir Jalil Razavi, Tuo Zhang, Xiao Li, Tianming Liu, and Xianqiao Wang

Role of Mechanical Factors on the Cortical Folding Development

Mir Jalil Razavi[1], Tuo Zhang[2,3], Xiao Li[3], Tianming Liu[2,*], and Xianqiao Wang[1,*]

[1]College of Engineering, University of Georgia, Athens, GA, USA
[2]Department of Computer Science and Bioimaging Research Center, University of Georgia, Athens, GA, USA
[3]School of Automation, Northwestern Polytechnical University, Xi'an, China

Deciphering mysteries of the structure-function relationship in cortical folding has emerged as the cynosure of recent research on brain. Understanding the mechanism of convolution patterns can provide useful insight into the normal and pathological brain function. However, despite decades of speculation and endeavors the underlying mechanism of the brain folding process remains poorly understood. This paper focuses on the three-dimensional morphological patterns of a developing brain under different tissue specification assumptions via theoretical analyses, computational modeling, and experiment verifications. The living human brain is modeled with a soft structure having outer cortex and inner core to investigate the brain development. Analytical interpretations of differential growth of the brain model provide preliminary insight into the critical growth ratio for instability and crease formation of the developing brain followed by computational modeling as a way to offer clues for brain's postbuckling morphology. Especially, tissue geometry, growth ratio, and material properties of the cortex are explored as the most determinant parameters to control the morphogenesis of a growing brain model. As indicated in results, compressive residual stresses caused by the sufficient growth trigger instability and the brain forms highly convoluted patterns wherein its gyrification degree is specified with the cortex thickness. Morphological patterns of the developing brain predicted from the computational modeling are consistent with our neuroimaging observations, thereby clarifying, in part, the reason of some classical malformation in a developing brain.

I. Introduction

Brain development and related cerebral convolution have been fascinating research topics for more than a century [1-3]. The grooves in the convoluted brain are called sulci and the ridges between them are called gyri. The outer layer of the brain is composed of folded gray matters, called the cortex, which is in turn made up of neuronal cell bodies and other support materials. The subcortex, or inner core, consists mostly of the white myelinated sheaths of neuronal axons [4]. Brain development is a sequence of complicated and convoluted processes starting from the growth of neuronal tubes, followed by neuronal proliferation, glial cell proliferation, neuronal migration and differentiation, axonal wiring, synaptogenesis, and myelination.

However, a comprehensive understanding of how those processes interactively accomplish the brain development still remains to be elucidated [5-7]. During the development, the cerebral

1

cortex experiences a noticeable expansion in volume and surface area accompanied by tremendous tissue folding [8,9]. Although there have been extensive studies on the brain folding over the past several decades, the mechanism of cortical folding is still ambiguous and debatable [10]. The most famous hypotheses in this area are related to the roles of radial growth, internal tension in neuronal fibers, and differential expansion of the cortex [10,11]. However, there are some evidences from experimental observations which contradict the first two hypotheses [10,12]. In the differential growth hypothesis, the outer layer of the brain is assumed to grow at a faster rate than the inner layer, acting as the driving mechanism of cortical folding [13]. Mismatch between growth rates of the layers engenders residual stresses which have been observed in a growing brain [14] and are believed to play a crucial role in the brain morphogenesis. Based on the differential growth hypothesis, several theoritical and computational studies have been conducted to reveal, in part, the cortical folding phenomenon, for example; buckling of an elastic surface on an elastic foundation [15], continuum mechanics-based model of growth [16], and 2D and 3D computational models [12,17,18]. In most previous studies related to the elastic buckling models of the brain, the elastic modulus of the outer layer was much higher than the core in order to produce buckling patterns which were not consistent with experimental observations [15,16]. In fact, the elastic modulus of the outer layer of cortex is not significantly different than that of inner regions of the brain [19-21]. A computational model of cortical convolution [18] suggested that without any additional assumption, the simple mechanical property of the cortex and differential growth is sufficient to produce cortical folding, which has been proven by other studies [11,13].

Recently, it has been shown that morphological abnormalities related to the cortex of the developing brain can be demonstrated by the mechanical model [22]. For example, Lissencephaly, which literally means "a smooth brain," is a rare brain formation disorder caused by imperfect neuronal migration characterized by the absence of normal convolutions in the cerebral cortex which [23-25]. A mechanical model with thick cortex and reduced growth in the cortical layer can identify specifications of this malformation [22]. Another example of brain abnormality is Polymicrogyria which surface of the brain normally has many folds. Either the whole surface (generalized) or parts of the surface (focal) can be affected [23,26]. A model with thin cortex and reduced growth in subcortical layer can mimic Polymicrogyria [22]. There are few reports on the 3D computational understanding of the brain morphology and its link to brain malformation. Therefore, study and research in this area is worthy of pursuit and may open new windows to diagnosis, treatment and therapy of severe disorders. The aim of this work is to investigate the growth and instability of a growing (cortex and core) 3D brain model, introduce a way to find the criteria for instability and gyrification, and link the gyrification patterns and their hinge types to the brain geometry and material property. Computational simulations are also performed in order to compare with the results from the analytical

approach and to predict secondary morphological patterns of the growing brain model. Finally, experimental observations are presented to validate the simulation results.

II. Methods

We use an analytical model to establish a primary intuition into crease formation of the developing brain and determine the critical growth for the onset of folding. Nevertheless, the analytical method cannot predict the evolution of cortical complex convolution after the critical point. Therefore, following the critical growth of the brain model, non-linear finite element models based on finite differential growth are employed to investigate the secondary morphological folds of the growing brain. Here we briefly introduce the the concept of each approach.

A. Analytical Method

A three-dimensional (3D) spherical model consisting of bilayer soft tissue (Fig. 1a) is constructed to explore the mechanism of cortical folding. The outer layer of the model represents the developing cortical plate of the brain (cortex) and the inner layer is considered as the core of the brain which is a simple organization of the subplate, intermediate zone and ventricular zone. Typically, cerebral cortex is a thin layer (2–4 mm)[10] in contrast to the core usually with a thickness of 50 mm. As mentioned in the Introduction section, the differential growth theory assumes that the cortex grows at a faster rate than the core of the brain, which is considered as the driving mechanism of cortical folding. Figure 1 provides the biological support of our 3D brain model. Flowchart in the Fig. 1(d) summarizes the mechanism of the diffrential growth from a biological viewpoint. Generally, radial glial cells (RGCs) with lower levels of Trnp1 can generate basal progenitors (BPs), also known as intermediate progenitors (IPCs), and basal radial glial cells (bRGCs). BPs can produce neurons while bRGCs provide additional guiding structures inducing faster neuron migration and finally resulting in considerable radial and lateral expansion, i.e. the convex folding pattern suggested in Refs [27,28]. Hence, the distribution difference of RGCs, at the cell level, regulates the cortical plate expansion by controlling the amount of migrating neurons. Based on the abovementioned biological mechanism, we can consider the outer layer of our model (cortex) grows faster than the inner layer (core) in our brain model.

We investigate the deformation, instability and gyrification of a cortex-core spherical brain model within the framework of finite elasticity. We use spherical coordinate systems; $X = (R, \Theta, \Phi)$ for the reference configuration and $x = (r, \theta, \varphi)$ for the grown and current configuration, Fig. 2.

Following the theory of multiplicative decomposition [29] , the deformation gradient, $F(X)$, is decomposed to a growth tensor $G(X)$ indicating the addition of materials, and an elastic deformation tensor $A(X)$ describing pure deformation resulting from stresses:

3

$$F = A \cdot G \qquad (1)$$

where $F = \partial x / \partial X$. The growth tensor maps a stress-free reference configuration to a grown stress-free state, and then the elastic deformation tensor maps the grown state to a stressed current state, Eq.(1). Although both G and A tensors may be incompatible deformations, their multiplication, F, should be a compatible deformation [29].

Without loss of generality, we assume that growth takes place only in the cortex of our brain model. For an isotropic growth, the growth tensor can be characterized by $G = gI$, where g ($g \geq 1$) is a constant and I is a unit tensor; for a tangential growth we consider there is no growth in the radial direction. Due to the spherical symmetry of our model, the elastic deformation tensor can be expressed for the isotropic growth as:

$$A = diag(\lambda_r, \lambda_\theta, \lambda_\varphi) \qquad \lambda_r = g^{-1} \partial r / \partial R, \quad \lambda_\theta = \lambda_\varphi = g^{-1} r / R \qquad (2)$$

and for the tangential growth as:

$$A = diag(\lambda_r, \lambda_\theta, \lambda_\varphi) \qquad \lambda_r = \partial r / \partial R, \quad \lambda_\theta = \lambda_\varphi = g^{-1} r / R \qquad (3)$$

In general, the elastic deformation of a living soft tissue yields a small amount of volume change; therefore, the nonlinear response of the living tissue can be described by an isotropic incompressible hyperelastic material. The incompressibility of the material implies that the determinant of the elastic deformation tensor should be equal to unit, i.e. $\det A = 1$. Here, to ensure incompressibility and hyperelasticity, a simple and common isotropic nonlinear neo-Hookean constitutive relationship is implemented

$$W = \frac{\mu}{2}(\lambda_r^2 + \lambda_\theta^2 + \lambda_\varphi^2 - 3) \qquad (4)$$

where μ is the shear modulus, and λ_r, λ and λ_φ are the radial and tangential principal stretches. Therefore, Cauchy stress σ can be related to the strain energy function by

$$\sigma = A \frac{\partial W}{\partial A} - pI \qquad (5)$$

where p is the hydrostatic pressure and I is a second-order unit vector. Mechanical equilibrium, without any body force, enforces the governing equation as:

$$div \, \sigma = 0 \qquad (6)$$

where "*div*" stands for the divergence operator in the current configuration. Due to the symmetry of our brain model, the deformation field after growth only depends $R, r = r(R)$. For simplicity, we assume that a fixed boundary condition is applied at $R = A = C/2$ in our brain model as shown in Fig. 2.

In order to find the critical growth ratio for instability, we follow the approach from our previous study on the crease formation of a biological tube due to growth in a confined environment [30]. Creases typically happen at the surface of a soft material without any hard skin in which an initially smooth surface forms a self-contacting shape with a sharp ridge or sulci [31]. The critical condition for the onset of crease formation in a compressed neo-Hookean soft material is

$$\lambda_r / \lambda_{\theta,\varphi} \geq 2.4 \qquad\qquad (7)$$

where λ_r is the ratio of the principal stretch in the radial direction while $\lambda_{\theta,\varphi}$ are the ratio of the principal stretches in the circumferential directions. This principle has been derived from a comparison of the elastic energy between in a creased body and in a smooth body [32]. In our bilayer brain model, the cortex grows faster than the core which acts as a confinement on the cortex. Mismatch between the growth rates of the cortex and core may induce compressive stresses. When this compressive stress exceeds a critical value, creases are expected to occur on the free surface of our model [30].

B. Numerical Method

After onset of instability in a developing brain model, in order to predict the secondary morphological change, computational models based on a non-linear finite element are carried out to complement the investigation from the analytical method. Both the cortex and core of the brain model are considered as hyperelastic neo-Hookean materials and the growth is mimicked via thermal expansion [33,34]. Self-contact property is added on the free surface of the cortex to reproduce the contact phenomenon while avoiding mesh penetration. A spherical hole is placed in the center of the model and a fixed boundary condition is applied. Since this fixed boundary is far enough from the surface of the cortex, its influence on the deformation pattern of the model can be negligible. Dynamic-Explicit solver in the commercial software Abaqus [35], which is suitable for large deformation, nonlinear, and quasi-static problems, is implemented to perform the secondary morphological changes in the brain model. Both the cortex and core of the brain model are meshed by a 3D stress, 8-node linear brick C3D8R element type with linear and quadratic viscosity of 0.06 and 1.2 in the dynamic step, respectively. Morphological patterns after instability in the brain model are not guaranteed to be exactly symmetric although the initial configuration is symmetric [36,37]. Robustness studies conclude that as long as the mesh size is small enough the qualitative features of the brain model do not depend on mesh size. The morphological pattern of the brain model also does not depend on the absolute value of shear moduli of the cortex and core but on the ratio of shear moduli. With the condition of incompressibility and Eq. (2), the growth rate of the cortex (g) for the isotropic growth case can be estimated from the volume ratio of the deformed system, V, to the undeformed system, V_0, $g_s{}^3 = V/V_0$.

III. Results

With the application of Eq. (1), along with governing equations and boundary conditions, deformation/stress fields, the growth criterion for instability, and the secondary morphology can be achieved. These analytical findings combined with the FE models are able to explain some unique mechanical characteristics of a developing brain.

A. Deformation and stress fields

Based on the Eq. (1) and its extension to the brain model in Fig.2, the deformation field of a growing brain model can be determined. For the case of isotropic growth, the growth tensor can be characterized by $\boldsymbol{G} = g\boldsymbol{I}$, where g ($g \geq 1$) is a constant and $\boldsymbol{I}$ is the unit tensor, so $g_r = g_\theta = g_\varphi = g$. The incompressibility condition implies the determinant of the elastic deformation tensor should be equal to unit, $\det \boldsymbol{A} = 1$. Therefore, for the isotropic growth of the brain model we can have

$$r^2 \partial r = g^3 R^2 \partial R \qquad (8)$$

By introducing $\bar{\bar{r}} = \frac{r}{A}, \bar{\bar{R}} = \frac{R}{A}, \bar{\bar{B}} = \frac{B}{A}, \bar{\bar{C}} = \frac{C}{A}$ and integrating Eq.(8), the deformation field for the core can be derived as

$$\bar{\bar{r}}^3 = 1 + g_c{}^3(\bar{\bar{R}}^3 - 1) \qquad 1 \leq \bar{\bar{R}} \leq \bar{\bar{B}} \qquad (9)$$

where g_c is the isotropic growth rate in the core. Following the similar way and the continuity condition at the interface of the cortex and core, we can have the deformation field of the cortex as follows

$$\bar{\bar{r}}^3 = 1 + g_c{}^3(\bar{\bar{B}}^3 - 1) + g_s{}^3(\bar{\bar{R}}^3 - \bar{\bar{B}}^3) \qquad \bar{\bar{B}} \leq \bar{\bar{R}} \leq \bar{\bar{C}} \qquad (10)$$

where g_s is the isotropic growth rate of the cortex. Without loss of generality, we assume that growth takes place only in the cortex, so $g_c = 1$, and Eq. (10) can be simplified as

$$\bar{r}^3 = 1 + g_s{}^3(\bar{R}^3 - 1) \qquad 1 \leq \bar{R} \leq \bar{C} \qquad (11)$$

where $\bar{r} = \frac{r}{B}, \bar{R} = \frac{R}{B}$ and $\bar{C} = \frac{C}{B}$. To find the normalized deformed outer radius of the cortex, $\bar{c} = \frac{c}{B}$, we should substitute the normalized initial outer radius of the cortex, $\bar{C}$, into Eq. (11).

Figure 3(a) depicts the normalized outer radius of the cortex after deformation under different isotropic growth rates. The initial thickness for the cortex is 2 ($T = C - B$) and the initial outer layer radius of the cortex (C) is 50 units [12]. $\bar{c}$ is a normalized value with $\bar{c} = c/B$, where B is the initial undeformed inner radius of the cortex showed in Figure 2.

From Figure 3(a) it can be clearly noticed that there is a very good agreement between the theoretical analysis and the finite element (FE) result for the deformation field of our brain model. From the FE model, after a critical growth rate the model loses stability and reaches to an irregular configuration. However, theoretical analysis cannot predict the evolution of cortical complex convolutions after the critical point for instability.

Figure 3(b) shows the normalized tangential stress (the ratio of the tangential stress to the shear modulus of the cortex) of the models under three different thicknesses of the cortex. We fix the isotropic growth rate of the cortex as $g_s = 2$ in all three models. Results point out that due to the growth of the cortex considerable compressive stresses are engendered through the cortex thickness. The thinner the cortex in the brain model is, the higher the compressive stress is. Also this compressive stress may play a crucial role in the instability of our brain model since several previous studies have shown that this kind of compressive stress in the free surface of soft materials leads to the formation of creases [30,32,33,36]. Before that, we need to answer what the critical growth rate of the cortex is for instability.

B. Instability and secondary deformation

Previous section has revealed that a compressive stress can be built up on the free surface of the cortex, thereby possibly resulting in creases [32]. Following Eqs. (7), (8), and (11), we can find the critical growth rate of the cortex for the case of isotropic growth

$$g_{crit} = [1/(1 - 7/12\bar{C}^3)]^{1/3} \qquad (12)$$

For the case of tangential growth, the critical growth rate for the cortex is

$$g^3{}_{crit}\bar{C}^3 - 2.4g^2{}_{crit}(\bar{C}^3 - 1) - 2.4 = 0 \qquad (13)$$

Figure 4 depicts the results from Eqs. (12) and (13), in which the critical growth rate depends on the initial geometry of the model, especially the thickness of the cortex.

As shown in Figure 4, with respect to the isotropic growth case, beyond a critical value of the outer radius of the cortex, $\bar{C} \cong 1.2$, instability does not occur no matter what the growth ratio of the cortex to core is. Similar phenomenon has been observed experimentally in a bilayer tissue model [37]. In other words, it means that a growing brain with a thick cortex is more stable than one with a thin cortex. With the decrease of the cortex thickness, the critical growth ratio for instability decreases, and $g \geq 1.34$ is required to start instability for a brain model with a very thin cortex which means from the analytical viewpoint the cortex should grow at least 1.34 times faster than the core to generate cortical folding. In contrast, with respect to the

case of the tangential growth, instability always happens in the brain model once it reaches the critical growth irrespective of the thickness ratio of the cortex to core. In the model with a thin cortex, the critical growth ratio for starting instability in both tangential and isotropic growth cases are very close to each other as shonw in Figure 4. Also we have made a comparison of the critical growth ratio in the cortex for instability between the results from analytical methods and FE models, which shows a good agreement with each other. .

Beyond instability, we can carry out a series of non-linear FE models with different thicknesses and material properties of the cortex and core to capture the morphological evolution of the brain model during the gyrification process. For the sake of computational efficiency and based on the symmetry of our brain model, a half spherical model is adopted in our FE analysis. For example, Figure 5 shows the morphological evolution of the brain model during the gyrification process with a set of special parameters, $\bar{C} = 50/48 \approx 1.042$ and $\mu_{cortex}/\mu_{core} = 2$. It can be observed that after a critical growth ratio the brain model starts to deviate from the spherical shape as depicted in Figure 5(a), indicating the model loses its stability and enters a new configuration with developed folds. With the continuation of growth, folds start to become more convoluted and go deeper inside the brain. Simulation results indicate that the gyrification pattern from our brain model is very similar to the real brain, although it should be kept in mind that the real gyrification of the brain is a sequence of complicated processes which starts from the growth of neuronal tubes, followed by neuronal proliferation, glial cell proliferation, neuronal migration and differentiation, axonal wiring, synaptogenesis, and myelination [5].

C. Effect of cortex thickness

Figure 4 has showed that the thickness of the cortex is a crucial parameter in the determination of critical growth ratio for instability in a growing brain model. Therefore, it can be expected that the cortex thickness exerts a positive effect on the morphological patterns of the brain after instability. With this regard, Figure 6 shows the morphological evolution dependency on the thickness of the cortex in the brain model. The left column of Figure 6 for the thin cortex $(T/C = 1/50)$ shows the formation of numerous small gyri and sulci after instability on the brain model. Recently, it has been shown that morphological abnormalities related to the cortex of the developing brain can be demonstrated by the mechanical model [22]. In the polymicrogyria malformation, the surface of the brain normally has many folds and the cortex thickness is thinner than one in a healthy brain. Either the whole surface (general) or parts of the surface (local) can be affected [23,26], as seen in Figure 2 of the reference [38]. Another evidence which may prove a thinner cortex leads to more creases is central sulcus, a primary somatosensory cortex which roughly consists of Brodmann areas #1, 2 and 3, and visual cortex [39]. The central sulcus and the primary visual cortex are the thinnest parts in the cortical region of the human brain [40]. By visual observation, central sulcus might be one of the

deepest sulci in brain and primary visual cortex has the most complicated folding patterns among all cortical cortex regions [41-43]. On the other hand, for the start of instability in the model with thick cortex a larger critical growth ratio is needed. As shown in right column of Figure 6, for the case with a thick cortex ($T/C = 3/50$), the number of folds is less than the normal one and the thickness of gyri is higher. This phenomenon has been observed in Lissencephaly, a malformation of the brain resulting in a thicker cortex than normal [23,24], as seen in Figure 1 of the reference [44]. These results show that cortex thickness has a crucial effect on the healthy development of the brain.

D. Effect of material properties

In addition to the geometrical parameters, the material property of the brain model may also play a vital role in the convolution pattern of the brain. In previous analytical derivations we assumed that the material properties of the cortex and core are the same or in some FE models the cortex is two times stiffer than the core. However, until now it is still very difficult to characterize brain matter mechanical properties accurately, because characterization of brain tissue is highly dependent on the definitions, tools, and procedures used [19]. The shear moduli of the cortex (grey matter) and core (white matter) have been reported differently in various studies [17,22,45,46]. Therefore, there is no firm and proven data for the relative material properties between grey and white matter. Hence, we want to show morphological evolution sensitivity to the relative shear modulus between the cortex and core rather than the absolute magnitude of shear moduli. Figure 7 shows the evolution of a developing brain with different material properties for the cortex and the core under the same geometric configuration, $T/C = 2/50$. Shear modulus ratio of cortex to core is considered to be 1, 2, and 4. Result shows difference between the shear moduli of the cortex and core has a great influence on the patterns of the developing brain model after instability. The brain model with a small shear moduli ratio prefers to develop creases first after instability; however, when the shear moduli ratio is large, the brain model prefers to wrinkle first and then develop creases. This finding reveals that, for the formation of creases in the brain, the shear moduli of the cortex and the core should be close to each other. This result shows that a change of the stiffness in the cortex or core of the brain caused by abnormalities or disorders may lead to a change in the pattern of the formation of gyri and sulci.

IV. Discussions

By the measurement in the real brain, we observe the same dependency of gyri thickness on the cortex thickness. Figure 8(a) is a neuroimage from the real adult brain with different special areas which show different cortical thicknesses. Dashed line in the Figure 8(b) connects the gyri thickness to the cortical thickness in the mentioned areas. It can be seen that the area with thick cortex (such as pre-central gyrus) forms thick or large gyri while the area with thin cortex

9

(such as post-central gyrus) forms thin or small gyri. This trend was observed in the FE model results, see Figure 6.

As can be inferred from Figure 8(b), gyri thickness is closely related to the cortex thickness. If gyri thickness in the FE models is roughly calculated and compared with the wave length of a buckling stiff layer on a soft substrate from a theoretical viewpoint, a similar trend and results are observable. The wavelength λ of the wrinkling pattern predicted by linear buckling theory is $\lambda = 2\pi t[\mu_f/3\mu_s]^{1/3}$, where t is the thickness of the film and μ_f and μ_s are the shear moduli of the film and substrate respectively [47]. From a theoretical viewpoint there is a linear relationship between wavelength (in the FE models referred as gyri thickness) and thickness of the film which is the same as the result of the FE models. Our results also reveal that a linear relationship may be considered between amplitude of gyri and cortical thickness, as from a theoretical view the amplitude of the wrinkles varies linearly with the thickness of film [48].

Another interesting result of convoluted models is the formation of special type of hinges same as in the real brain. It has been reported that cortical gyral folding pattern can be effectively described by the hinges number [49]. In addition to the number of hinges on gyri, the shape of hinge line can also be used to describe the local cortical gyral folding pattern [50]. In the first row of Figure 9, we show three different patterns of three hinges in the convoluted models. Curves on the convoluted models represent the crest lines in the 'gyral' regions. Those three-hinge patterns can find their counterparts in real cerebral cortical surfaces (see the second row of Figure 9). Those cortical surfaces were reconstructed on the boundaries between gray matters and white matters obtained based on T1-weighted MRI segmentation from our previous study [51]. Similarity between the three-hinge patterns in convoluted models and their real-world counterparts can be appreciated by visual examination.

V. Conclusion

In this paper, we have investigated the instability and morphological evolution of a developing brain with an integrated analytical and computational methodology. Critical growth ratios for instability in the brain model have been derived both analytically and numerically. Results show that the thickness of the cortex and the relative material properties of the cortex to core of the brain play critical roles in the determination of the secondary morphological patterns of the developing brain model. Finally, the present study along with other neuroimaging findings can be used as a tool to clarify some malformations in a developing brain.

Corresponding authors: Xianqiao Wang (xqwang@uga.edu) and Tianming Liu (tliu@uga.edu).

References

[1]   W. E. L. G. Clark, Deformation patterns in the cerebral cortex (Printed at the Oxford University Press by John Johnson, 1945).
[2]   K. Zilles, E. Armstrong, A. Schleicher, and H.-J. Kretschmann, Anat. Embryol. **179**, 173 (1988).
[3]   J. Rogers et al., NeuroImage **53**, 1103 (2010).
[4]   T. Paus, Brain and cognition **72**, 26 (2010).
[5]   D. C. V. Essen, Nature **385**, 313 (1997).
[6]   E. S. Monuki and C. A. Walsh, Nat. Neurosci. **4**, 1199 (2001).
[7]   E. A. Grove and T. Fukuchi-Shimogori, Annu. Rev. Neurosci. **26**, 355 (2003).
[8]   G. Roth and U. Dicke, Trends. Cogn. Sci. **9**, 250 (2005).
[9]   K. Zilles, N. Palomero-Gallagher, and K. Amunts, Trends Neurosci. **36**, 275 (2013).
[10]   P. Bayly, L. Taber, and C. Kroenke, J. Mech. Behav. Biomed. Mater. **29**, 568 (2014).
[11]   L. Ronan et al., Cereb. Cortex, bht082 (2013).
[12]   T. Tallinen, J. Y. Chung, J. S. Biggins, and L. Mahadevan, Proc. Natl. Acad. Sci. USA. **111**, 12667 (2014).
[13]   P. Bayly, R. Okamoto, G. Xu, Y. Shi, and L. Taber, Phys. Biol. **10**, 016005 (2013).
[14]   G. Xu, P. V. Bayly, and L. A. Taber, Biomech. Model. Mechanobiol. **8**, 253 (2009).
[15]   D. P. Richman, R. M. Stewart, J. W. Hutchinson, and V. S. Caviness Jr, Science **189**, 18 (1975).
[16]   R. Raghavan, W. Lawton, S. Ranjan, and R. Viswanathan, J. Theor. Biol. **187**, 285 (1997).
[17]   S. Budday, P. Steinmann, and E. Kuhl, J. Mech. Phys. Solids. **72**, 75 (2014).
[18]   R. Toro and Y. Burnod, Cereb. Cortex **15**, 1900 (2005).
[19]   S. Chatelin, A. Constantinesco, and R. Willinger, Biorheology **47**, 255 (2010).
[20]   M. T. Prange and S. S. Margulies, J. Biomech. Eng. **124**, 244 (2002).
[21]   J. Van Dommelen, T. Van der Sande, M. Hrapko, and G. Peters, J. Mech. Behav. Biomed. Mater. **3**, 158 (2010).
[22]   S. Budday, C. Raybaud, and E. Kuhl, Sci. Rep. **4**, 5644 (2014).
[23]   T. Pang, R. Atefy, and V. Sheen, The neurologist **14**, 181 (2008).
[24]   C. Raybaud and E. Widjaja, Neuroimaging. Clin. N. Am. **21**, 483 (2011).
[25]   W. Dobyns and C. Truwit, Neuropediatrics **26**, 132 (1995).
[26]   R. Guerrini, W. B. Dobyns, and A. J. Barkovich, Trends Neurosci. **31**, 154 (2008).
[27]   M. Götz and W. B. Huttner, Nat. Rev. Mol. Cell. Biol. **6**, 777 (2005).
[28]   R. Stahl et al., Cell **153**, 535 (2013).
[29]   E. K. Rodriguez, A. Hoger, and A. D. McCulloch, J. Biomech. **27**, 455 (1994).
[30]   M. J. Razavi and X. Wang, RSC Advances **5**, 7440 (2015).
[31]   B. Li, Y.-P. Cao, X.-Q. Feng, and H. Gao, Soft Matter **8**, 5728 (2012).
[32]   W. Hong, X. Zhao, and Z. Suo, Appl. Phys. Lett. **95**, 111901 (2009).
[33]   L. Jin, S. Cai, and Z. Suo, EPL. **95**, 64002 (2011).
[34]   Y. Cao, Y. Jiang, B. Li, and X. Feng, Acta. Mech. Solida. Sin. **25**, 483 (2012).
[35]   Abaqus analysis user's manual, Version 6.13, Dassault System Simula Corp, RI, USA, 2013.
[36]   T. Tallinen, J. S. Biggins, and L. Mahadevan, Phys. Rev. Lett. **110**, 024302 (2013).

[37]	J. Dervaux, Y. Couder, M.-A. Guedeau-Boudeville, and M. B. Amar, Phys. Rev. Lett. **107**, 018103 (2011).

[38]	B. Rai, R. Gouda, S. Moka, and L. E. Dunbar, J. Child. Neurol., 0883073814544367, doi: 10.1177/0883073814544367 (2014).

[39]	K. Brodmann and L. J. Garey, Brodmann's: Localisation in the Cerebral Cortex (Springer, 2007).

[40]	B. Fischl and A. M. Dale, Proc. Natl. Acad. Sci. USA. **97**, 11050 (2000).

[41]	P. Rakic, Science **241**, 170 (1988).

[42]	K. Im, J. M. Lee, U. Yoon, Y. W. Shin, S. B. Hong, I. Y. Kim, J. S. Kwon, and S. I. Kim, Hum. Brain Mapp. **27**, 994 (2006).

[43]	W. Welker, in Cereb. Cortex (Springer, 1990), pp. 3.

[44]	S. Sharma, P. Jain, and S. Aneja, IJEP. **1**, 49 (2014).

[45]	P. J. McCracken, A. Manduca, J. Felmlee, and R. L. Ehman, Magn. Reson. Med. **53**, 628 (2005).

[46]	S. A. Kruse, G. H. Rose, K. J. Glaser, A. Manduca, J. P. Felmlee, C. R. Jack Jr, and R. L. Ehman, NeuroImage **39**, 231 (2008).

[47]	X. Chen and J. W. Hutchinson, J. Appl. Mech. **71**, 597 (2004).

[48]	S. Yang, K. Khare, and P. C. Lin, Adv. Funct. Mater. **20**, 2550 (2010).

[49]	K. Li, L. Guo, G. Li, J. Nie, C. Faraco, G. Cui, Q. Zhao, L. S. Miller, and T. Liu, NeuroImage **52**, 1202 (2010).

[50]	X. Yu, H. Chen, T. Zhang, X. Hu, L. Guo, and T. Liu, in Biomedical Imaging (ISBI), 2013 IEEE 10th International Symposium on (IEEE, 2013), pp. 85.

[51]	T. Liu, J. Nie, A. Tarokh, L. Guo, and S. T. Wong, NeuroImage **40**, 991 (2008).
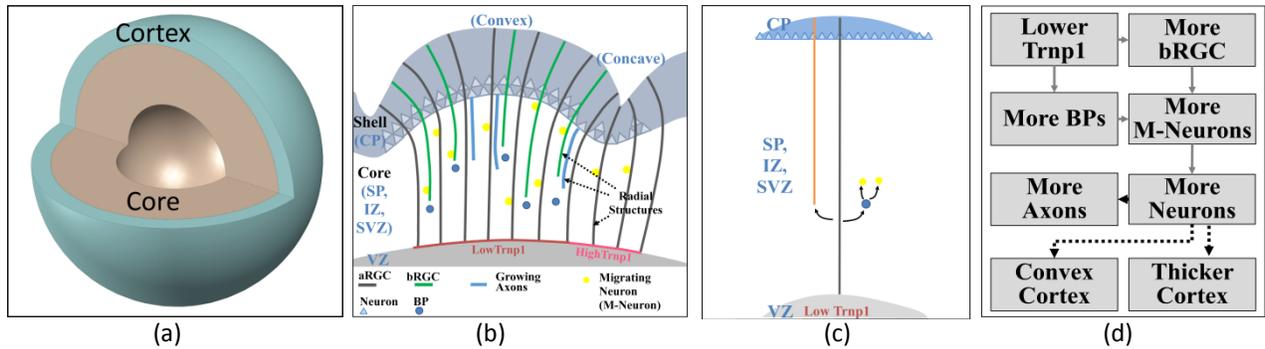
FIG. 1 (Color online). (a) An idealized spherical bilayer brain model; (b) and (c) biological foundation of neurogenesis we are interested in; (d) flow chart of how Trnp1 regulates the cortical folding pattern. The dashed line arrows suggest macro-scale features of the cortex. Abbreviations: aRGC, apical RGC; bRGC, basal RGC; BP, basal progenitor; CP, cortical plate; VZ, ventricular zone; SVZ, subventricular zone; SP, subplate; IZ, intermediate zone.
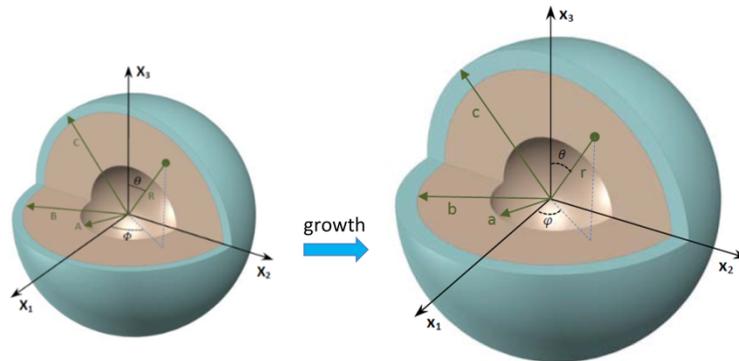
FIG. 2 (Color online). Growth of a spherical bilayer brain model from the initial configuration to current configuration.
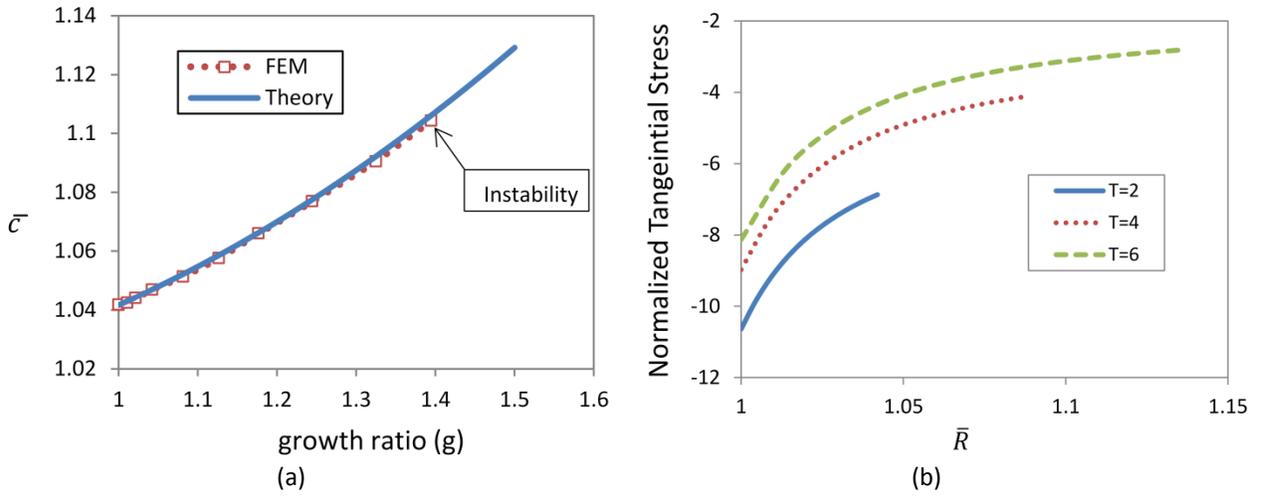
FIG. 3 (Color online). (a) Normalized deformation for the outer radius of cortex according to the isotropic growth ratios of cortex. Initial thickness of cortex is 2 and initial outer radius of cortex is 50 units. Cortex and core have the same material property. (b) Normalized tangential stress (σ/μ_s) distribution in the cortex with different thicknesses. Isotropic growth ratio for cortex of all models is $g_s = 2$.

15
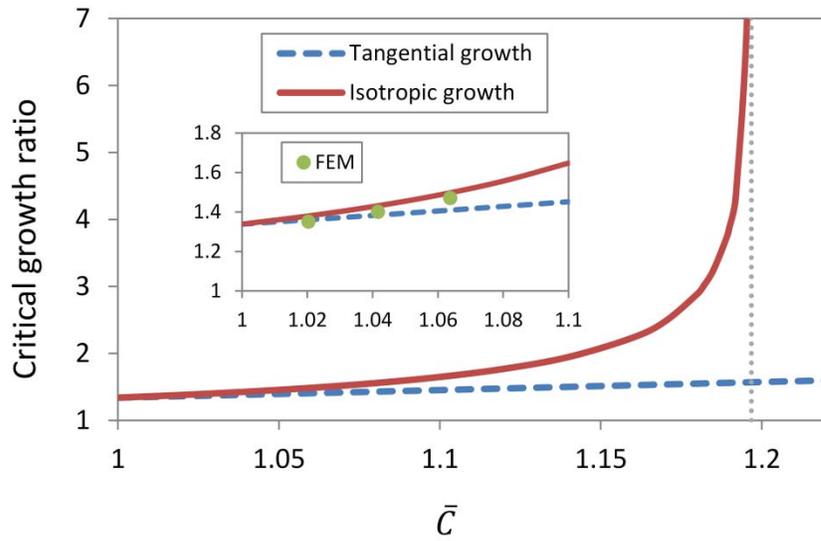
FIG. 4 (Color online). Critical growth ratio for starting instability for isotropic and tangential growth of cortex. $\bar{C}$ is the normalized value as defined $\bar{C} = C/B$, where C and B are the initial unreformed inner and outer radius of cortex.
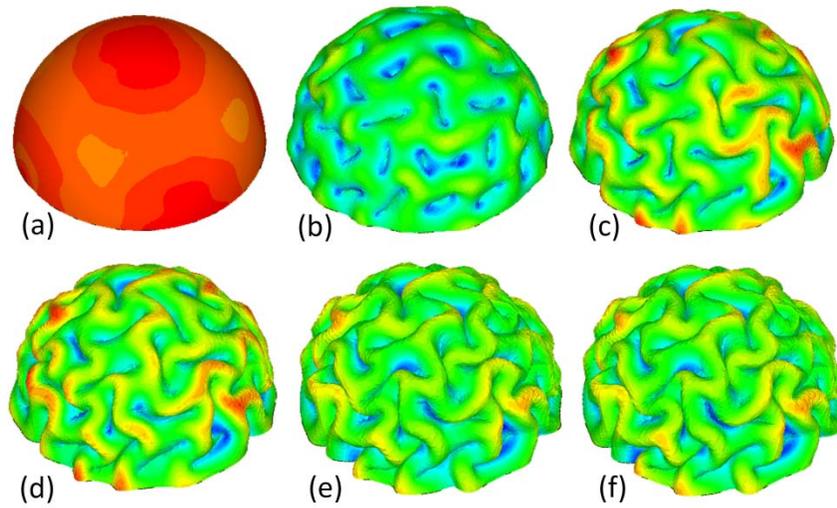
FIG. 5 (Color online). Morphological evolution steps for a growing bilayer spherical brain model; (a-f), initial thickness of cortex is 2 and initial outer layer of cortex (C) is 50 units. Contour shows displacement (figures are not in same scale).
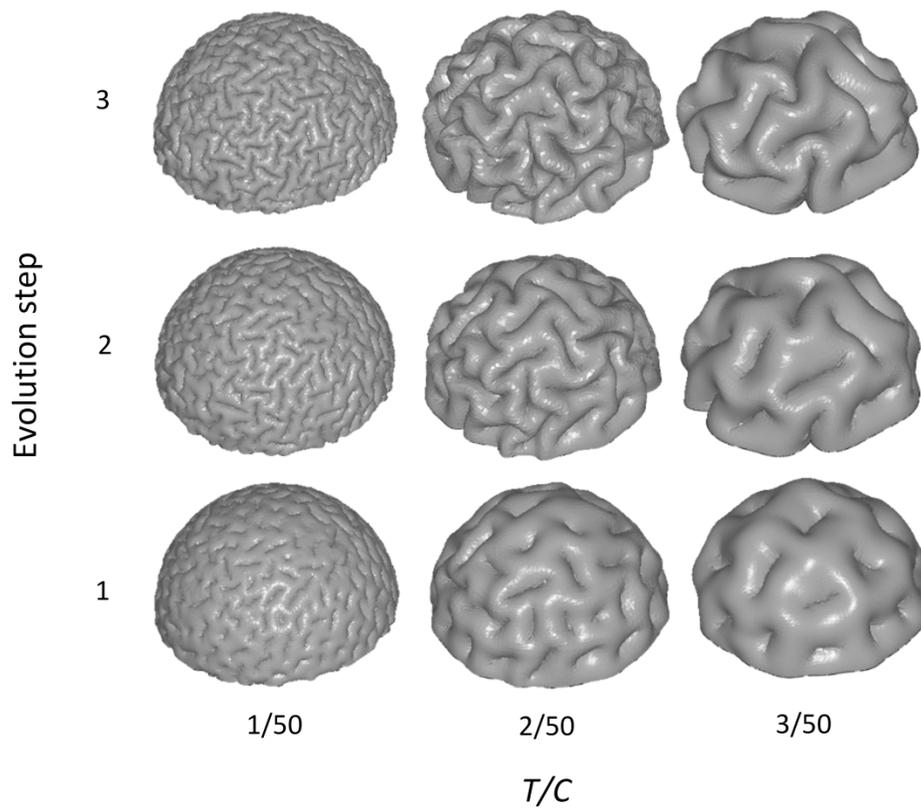
FIG. 6 (Color online). Morphological evolution of the growing model with different thickness of cortex, $\mu_{cortex}/\mu_{core} = 2$. Time steps from 1 to 3 show gyrification of models step by step (figures are not in same scale).
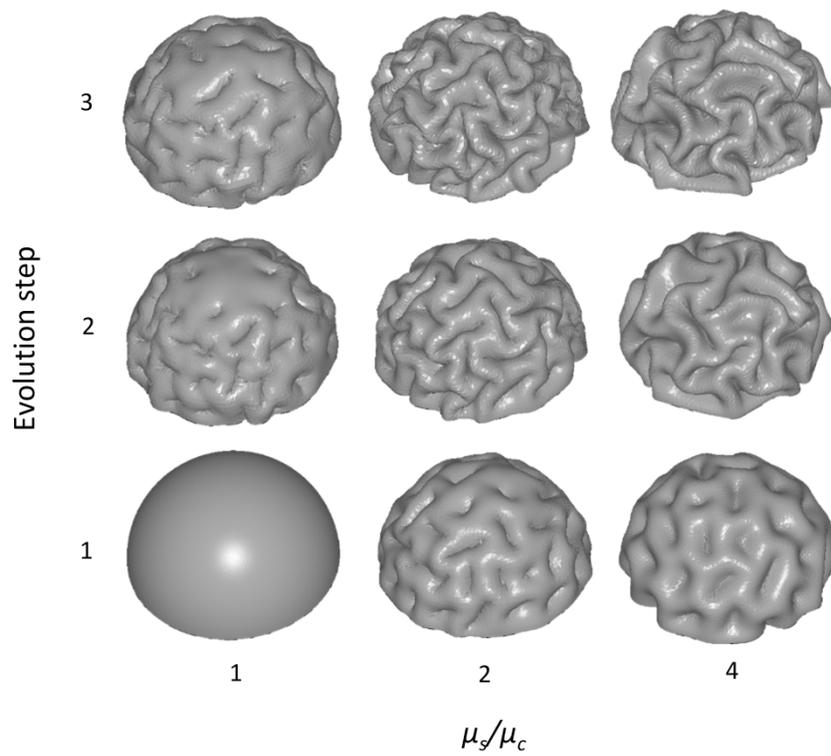
FIG. 7 (Color online). Morphological evolution of the growing model with different shear modulus ratio of cortex to core, ($T/C = 2/50$). Time steps from 1 to 3 show gyrification of models step by step (figures are not in the same scale).
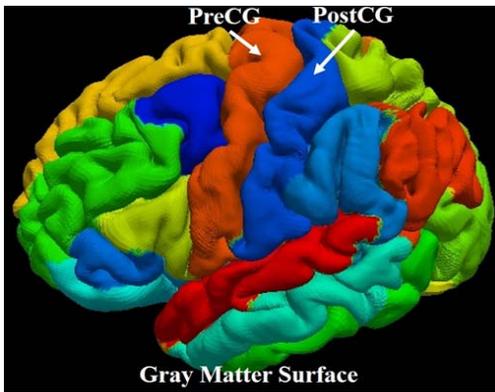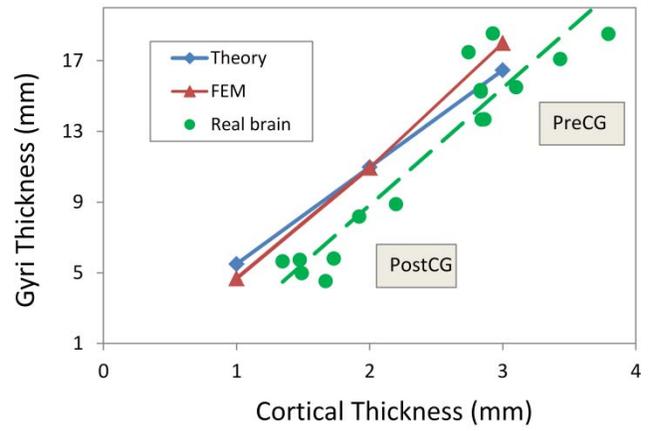
FIG. 8 (Color online). (a) Gyri annotation on adult brain gray matter surfaces, PreCG: pre-central gyrus; PostCG: post-central gyrus. (b) Dependency of gyri thickness to the thickness of cortex. Gyral thickness is measured on gray matter (cortex) surfaces.
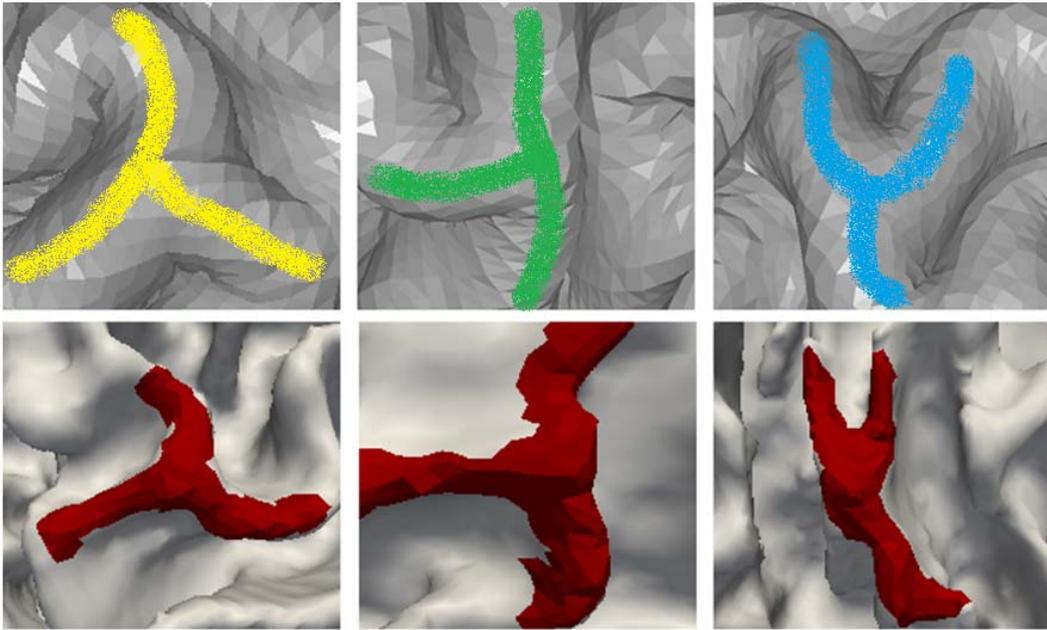
FIG. 9 (Color online). First row: Three examples of three hinges on convoluted models; second row: similar gyral folding patterns on white matter surface in real brains. Red color regions highlight the crests of gyral regions which are based on T1-weighted MRI segmentation (figures are not in the same scale).